International Journal of Pharmaceutics 418 (2011) 297–303

Contents lists available at ScienceDirect

International Journal of Pharmaceutics

journal homepage: www.elsevier.com/locate/ijpharm

Radial tensile strength prediction of relaxing and relaxed compacts by near-infrared chemical imaging

Benoît Igne, Carl A. Anderson*, James K. Drennen III

Duquesne University Center for Pharmaceutical Technology, 600 Forbes Avenue, Pittsburgh, PA 15282, USA

ARTICLE INFO

Article history:
Received 29 October 2010
Received in revised form 26 April 2011
Accepted 14 May 2011
Available online 20 May 2011

Keywords:
Near-infrared chemical imaging
Viscoelastic relaxation
Radial tensile strength
Quality attributes

ABSTRACT

The prediction of radial tensile strength (RTS) of relaxing solid dosage forms by near-infrared hyperspectral chemical imaging was studied. Compacts consisting of starch, lactose, and a mixture of four components were created at different compression forces to develop density models. Predicted density distribution parameters were subsequently used to estimate RTS. Chemical images were collected shortly after compression, repeated every 30 min for 2 h, and a final image was collected after 2 weeks. A two step process, involving first the prediction of compact density at each pixel (using a partial least squares model) and second the relationship between compact density distributions and RTS was implemented. Among the parameters with a significant relationship with RTS, the median of the distribution of density predictions in an image was identified as a robust parameter. Coefficients of determinations for this prediction ranged from 0.96 to 0.99 were obtained with a maximum error in validation of 0.10 MPa for the four-component formulation compacts. The prediction of RTS of fully relaxed compacts from spectral data collected on relaxing compacts was demonstrated. These results demonstrate the potential to use near-infrared chemical imaging in real-time to predict RTS values of fully relaxed compacts.

1. Introduction

The determination of critical quality attributes (CQA) of pharmaceutical dosage forms immediately following compression is an important part of achieving real-time controlled release. Both chemical and physical properties must be monitored and controlled for solid dosage forms. Thus, physical characteristics such as tablet density and hardness must be determined (in addition to chemical tests such as content uniformity and assay) to ensure adequate dosage form performance.

The effect of tablet aging has been documented in the literature with respect to mechanical strength, disintegration, and dissolution times (Rees and Shotton, 1970; Alam and Parrott, 1971; Lowenthal, 1972; Lordi and Shiromani, 1984; Karehill and Nystrom, 1990; Gordon et al., 1993). Aging is typically attributed to mechanical relaxation following uniaxial compression. The magnitude of these changes varies as a function of the relative ratio of material having elastic and viscoelastic behaviors under compression. Brittle elements will tend to immediately release their stored elastic energy upon removal of stress. On the contrary, materials responding to stress by plastic deformation tend to recover via viscoelastic relaxation, where elastic energy stored during compression is released more slowly over time (David and Augsburger, 1977).

These powder behaviors pose a significant challenge when considering real-time release. Indeed, the on-line measurement of tablet physical properties using a secondary method can be difficult when the goal of the analysis is prediction of CQAs of fully relaxed tablets based on information gathered on relaxing compacts. Thus, developing approaches to predict the properties of relaxed compacts is of significant interest.

The last two decades have brought significant development to process analytical technologies for the analysis of pharmaceutical products off-line, at-line, and on-line (Bakeev, 2005). Among the numerous process monitoring methods available, near infrared spectroscopy has been widely used to monitor pharmaceutical manufacturing processes (Cogdill et al., 2004; Roggo et al., 2004, 2007; Parris et al., 2005; Swarbrick et al., 2005; Shi et al., 2008; Sarraguca and Lopes, 2009). This spectroscopic technique is rapid and non-destructive, and is based on the absorption of near infrared light by organic molecules as a function of their chemical and physical properties in the sample of interest.

More recently, hyperspectral chemical imaging has been used to monitor both chemical and physical properties in tablets (Reich, 2005; Gendrina et al., 2008; Gowen et al., 2008; Ellison et al., 2008). Chemical imaging presents the advantage of spatial resolution of spectra that allows for local characterization of pharmaceutical products as well as potential new sampling strategies for high

* Corresponding author. Tel.: +1 412 396 1102; fax: +1 412 396 1608.
E-mail address: andersonca@duq.edu (C.A. Anderson).

0378-5173/$ – see front matter © 2011 Elsevier B.V. All rights reserved.
doi:10.1016/j.ijpharm.2011.05.038

throughput tablet monitoring systems. Indeed, some imagers can gather in a few frames (collected in less than a second) the near-infrared spectra of multiple tablets. Thus, with the objective of real-time release, chemical imaging provides significant potential as a measurement system in a manufacturing environment.

Among the physical properties to which near-infrared spectroscopy is sensitive, force to tensile failure, has been studied as a surrogate for hardness (Morisseau and Rhodes, 1997; Ebube et al., 1999; Guo et al., 1999; Kirsch and Drennen, 1999; Donoso et al., 2003; Gustafsson et al., 2003; Tatavarti et al., 2005; Blanco and Alcalá, 2006a; Blanco et al., 2006b; Otsuka and Yamane, 2006; Wu et al., 2006; Short et al., 2009). Hardness is, in turn, frequently a substantial predictor of the performance of the dosage form in patients. However, it is typically not practical to measure it as a routine quality control test via micro-indentation measurements (Cao et al., 2010). Unfortunately, the more common and practical measurement of force to tensile failure, is highly dependent on the dimensions and shape of a tablet. In an attempt to generalize measurements, radial tensile strength (RTS) was developed to allow comparison between compacts of different dimensions and geometries (Fell and Newton, 1970). For cylindrical flat-faced tablets, RTS is calculated as follows:

$$\mathrm{RTS} = \frac{2F}{\pi D t} \quad (1)$$

where F is the force to tensile failure, D is the diameter, and t is the thickness of the compact.

In this present article, the ability to predict RTS from near-infrared chemical images was investigated. The chemical imaging signal of both relaxing and fully relaxed compacts was used as a means to investigate the capability to predict, at-line, RTS of fully relaxed compacts. This study represents a first step toward the implementation of chemical imaging for on-line measurements of compact critical quality attributes.

2. Materials and methods

2.1. Compacts

Compacts of Starch 1500 (Colorcon, West Point, PA, USA), lactose monohydrate (Foremost Farms, Rothschild, WI, USA), and a four-component formulation containing theophylline anhydrous (Knoll A.G., Ludwigshafen, Germany), microcrystalline cellulose (Avicel PH-200, FMC BioPolymer, Mechanicsburgh, PA, USA), Starch 1500, and lactose monohydrate (25% (w/w) for each constituent) were manufactured. Eight compacts were created for each material. Three were subsequently used for model calibration and five for validation. An Instron Universal Testing System (Model 5569; Instron Corp.; Norwood, MA, USA) with a 50-kN load cell was used to prepare the compacts while simultaneously measuring the applied force and punch displacement. Compacts weighing approximately 500 mg were prepared in a 10-mm cylindrical die using flat-faced punches and applied forces of 10, 14.1, and 20 kN (for calibration set) with a crosshead speed of 10 mm min^{-1}. Validation compacts were compressed at 10, 11.9, 14.1, 16.8, and 20 kN (linear in log scale). Compaction forces were similar for all materials. Decompression was initiated immediately upon reaching the maximum applied load for each compact (dwell time = 0 s). Powders were left to reach equilibrium in a humidity chamber with a saturated sodium chloride solution prior to compression (35.5% relative humidity). Compacts were also stored in the same conditions after image collection. The four-component formulation was blended in a jar mill for two 5-min periods, prior to compression.

While the total number of samples might seem low, the large variability in local density present on each compact is expected to represent the range that would be observed with additional compacts. In addition, the spectra collected at each pixel of a chemical image can be considered elements of an independent population. Some spatial correlation exists, but the scale is limited to a few pixels. Thus, as will be described later, each compact, from which 81920 spectra are collected, represents substantial variability in local density and spectral variance. The large amount of data and variance available per compact was considered sufficient to represent the variability that additional compacts would bring.

2.2. Chemical image collection

MatrixNIR™ chemical imaging system (Malvern Inc., Olney, MD, USA), a focal-plane array based global imaging system, was used to collect images for all the compacts. Each image contained 256 by 320 pixels. A 0.5× objective (field of view: 17.2 mm by 21.5 mm) was used. The hyperspectral data were collected over the spectral range of 1000–1700 nm with a 5 nm wavelength interval and a total of 16 co-adds at each wavelength.

After compression, compacts were imaged every 30 min for 2 h (total of 4 images). The first image was taken 20 min after compression as time was necessary to make physical measurements on the compacts. The position of the compacts in the field of view was maintained stationary between image collections. Two weeks after compression, a final image was taken and the compact was crushed within 2 h.

2.3. Radial tensile strength prediction methodology

The use of chemical imaging for at-line/on-line applications requires the development of optimization techniques that will reduce the quantity of data and provide information for decisions with interpretable results. In the present study, the characteristics of the distribution of the density information within each compact were used as independent variables to predict RTS.

Apparent density (ratio of mass to volume) was measured using a micrometer after compression, image collection, and before RTS measurement for each compact (Table 1). A calibration model for density was developed using the three calibration compacts for each material. The model was developed using partial least squares (PLS) with mean centered spectral data and autoscaled (mean zero, unit variance) apparent density values. This step reduces the dimensionality of the data from three (256 by 320 by 141 hypercube) to two (256 by 320 image plane). Density distribution parameters (first to fourth moments) were then calculated, along with other statistics of the populations. Moments (mean, variance, skewness, and kurtosis) and median, first and third quartiles and percentiles (2.5 and 97.5%) were used in a multiple linear regression (MLR) to relate density distribution information to RTS. Ultimately, the number of data points considered in the evaluation of a compact was reduced by a factor of ~1.2 million, allowing real-time quality assessment. The calibration models were tested using five additional validation compacts. Models were independently developed for each formulation, using a two-step procedure. First, density values were predicted by the density model developed in calibration. Second, predicted density distribution characteristics were determined and subsequently used as input for the MLR model to predict RTS. Fig. 1 summarizes the process.

Density information collected immediately after compression, after image collection (1 h 50 min after compression), and 2 weeks later was used to develop individual calibration models to predict equilibrium RTS for tablets relaxing via different relaxation mechanisms. Force to failure used in RTS calculations was determined by the same Instron Universal Testing System, equipped with a 1-kN load cell and a crosshead speed of 10 mm min^{-1}.

All calculations were performed using MATLAB 2010a (The Mathworks Inc., Natick, MA, USA) and the PLS_Toolbox 5.8 (Eigen-

Table 1
Density measurements for relaxing and relaxed compacts (mg mm^{-3}).

Comp force (kN)	Calibration			Validation				
	10	14.1	20	10	11.8	14.1	16.8	20
Starch 1500								
20 min	1.1387	1.1964	1.2782	1.1141	1.1608	1.1881	1.2197	1.2629
1 h 50 min	1.1215	1.1831	1.2652	1.1057	1.1487	1.1749	1.2089	1.2403
2 weeks	1.1159	1.1774	1.2548	1.0877	1.1385	1.1660	1.2017	1.2357
Lactose mono								
20 min	1.2875	1.3150	1.3523	1.2778	1.3059	1.3146	1.3332	1.3526
1 h 50 min	1.2811	1.3135	1.3492	1.2744	1.3011	1.3095	1.3303	1.3501
2 weeks	1.2786	1.3074	1.3426	1.2692	1.2998	1.3027	1.3291	1.3485
4-Comp form								
20 min	1.2232	1.2845	1.3406	1.2232	1.2582	1.2894	1.3144	1.3429
1 h 50 min	1.2184	1.2823	1.3347	1.2140	1.2538	1.2882	1.3020	1.3301
2 weeks	1.2157	1.2808	1.3329	1.2112	1.2492	1.2867	1.2995	1.3273

vector Research, Inc., Manson, WA, USA). JMP 8 (SAS, Cary, NC, USA) was used to develop MLR models.

3. Results and discussion

3.1. Density models and prediction distribution

The prediction of RTS from density distribution statistics first required the creation of prediction models for density. Using calibration compacts, PLS models were developed for each formulation (spectra from each compact were associated with the measured apparent density). These models were then used to predict the density at each pixel of the validation compacts. The number of latent variables used to develop prediction models for starch, lactose, and the mixture was four. The number of latent variables was determined as a function of the variance explained and the trends of calibration and cross-validation errors. The local variability in the densities present within each compact required four latent variables to adequately capture the variance of the system.

Fig. 2 shows predicted density images of relaxing compacts for starch (Fig. 2a–j), for lactose (Fig. 2k–o), and for the theophylline formulation (Fig. 2p–t). While only one chemical species was present in the compacts of lactose and starch, variability in density distributions was clearly observed within each compact. This was consistent with previous reported results (Gendrina et al., 2008).

Differences existed between the density profiles predicted using apparent density measured after compression and 2 weeks later (Fig. 2a–j). This was also valid for lactose and the four-component formulation (data not shown). This observation illustrated the need to develop standardized practices for calibration and validation of density models as relaxation timing had a significant impact on the predicted values, which subsequently impact RTS predictions.

Density trends observed for lactose compacts were similar, but on a much reduced magnitude as most of the relaxation took place immediately after compression and before the image collection procedure could be completed (Fig. 2k–o). The relaxation patterns for the four-component formulation were more pronounced than those observed for starch and lactose; the combination of elastic and viscoelastic relaxation creating unique aging behaviors (Fig. 2p–t).

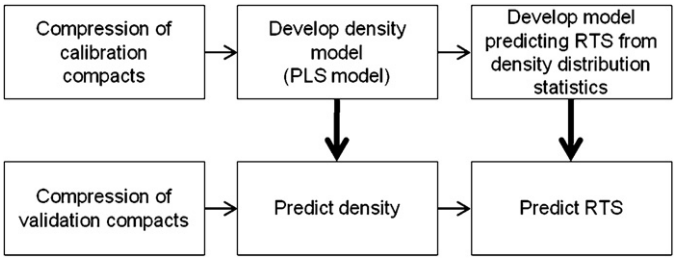

Fig. 1. Flow of the process used to generate and analyze the data.

Fig. 3 shows box plots of the distribution of densities 2 weeks after compression for each of the starch compacts presented in Fig. 2 (starch compact compressed at 10 kN, 11.9 kN, 14.1 kN, 16.8 kN, and 20 kN; apparent density measured after relaxation). Means and median were similar and a linear relationship existed between compression force and the mean and median of each distribution. Mean predicted densities differed from measured densities (Table 1), especially at high compression forces. While a good agreement was observed from 10 to 14.1 kN, other distributions presented a larger bias. This corresponded with a noticeable increase in the number of values that exceeded a 99% confidence interval. A possible explanation for this is the fact that larger compression forces generated more extreme relaxation phenomena creating more variability within each compact. Further, the extreme compression values may exhibit subtly different compression and relaxation mechanisms.

Table 2 presents the distribution statistics calculated from the PLS model predictions at each time point for the validation compact of starch compressed at 14.1 kN. The upper part of the table corresponds to the use of density of the final compacts as the calibration dependent variable and the bottom part corresponds to the density measured 20 min after compression. While the shift in distribution was significant between each time point ($\alpha = 0.05$), due to the overwhelming degrees of freedom (about 26,000 corresponding to the number of data points available), the most noticeable elements were that while the mean and median remained rather constant, the standard deviation increased with relaxation time. The mean and median of predicted density was consistent with values of apparent density determined by the micrometer (Table 1). This was true for all three formulations used (data not shown). Thus, the mean and median predicted density appeared to be robust estimators as they did not undergo substantial changes during relaxation. However, a significant difference existed when comparing with density profiles observed 2 weeks after compression ($\alpha = 0.05$). This difference was significantly larger when using density of fully relaxed compacts as dependent variable in the PLS calibration model ($\alpha = 0.05$).

3.2. Linear regression predictions of RTS from predicted density distribution statistics

A stepwise regression approach was used to identify density statistics with a significant relationship to RTS ($\alpha = 0.05$). The mean or the median were the only two variables significantly correlated

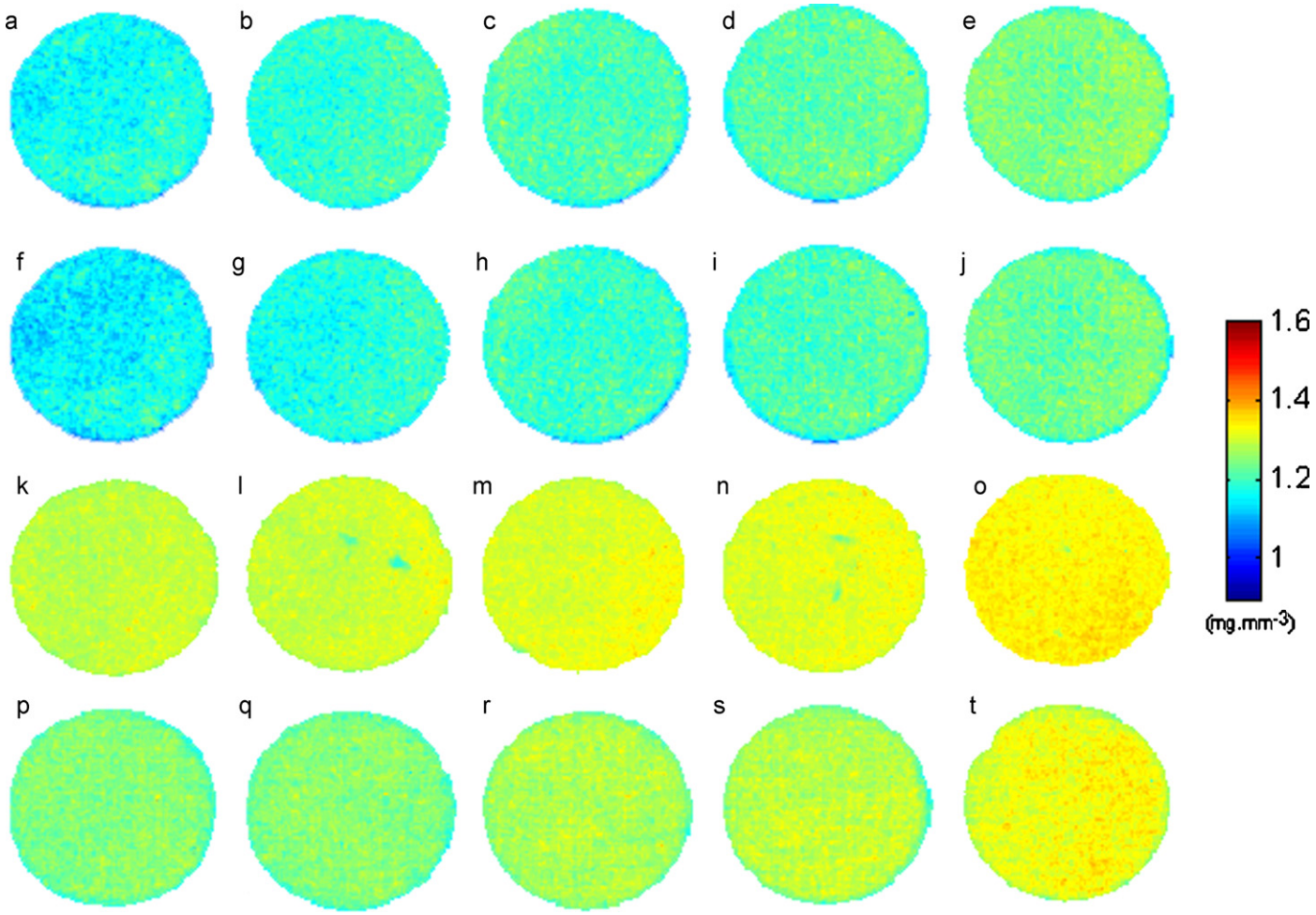

Fig. 2. Density prediction images of starch compacts. Compacts (a, f, k, and p) were compressed at 10 kN, compacts (b, g, l, and q) at 11.9 kN, (c, h, m, and r) at 14.1 kN, (d, i, n, and s) at 16.8 kN, and (e, j, o, and t) at 20 kN. Predictions of compacts a–e were generated from a partial least squares model using density measurement as dependent variable made 20 min after compression. Predictions of other compacts were generated from a partial least squares model using density measurement as dependent variable made 2 weeks after compression.

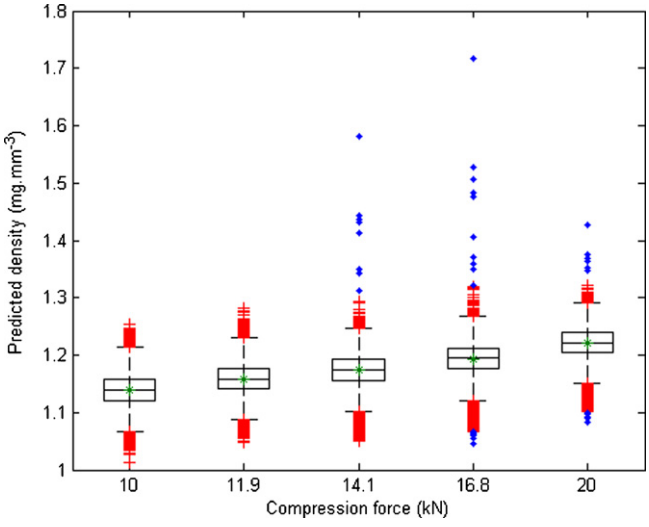

Fig. 3. Box plot of the predicted density distributions of validation starch compacts. Outliers are represented by red crosses while values outside the 99% confidence interval are displayed as blue dots. (For interpretation of the references to color in this figure legend, the reader is referred to the web version of the article.)

to RTS. Because of the robust nature of the median compared to the mean (less sensitive to outliers), the median was used in the subsequent calculations. A least-squares fit was then used to relate the median of each density distribution from the calibration sets to RTS values. The linear fit between median and RTS determined for calibration samples were then used to predict RTS of validation compacts. Fig. 4 presents the validation results for all three materials (relaxing compacts only – from 20 min to 1 h 50 min relaxation).

For starch, coefficients of determination (r^2) between 0.92 and 0.98 were observed, along with a maximum root mean square error of prediction (RMSEP) of 0.16 MPa. For lactose, r^2 ranged from 0.96 to 0.99, with a maximum RMSEP of 0.11 MPa. Finally, for the four-component formulation, r^2 ranged also between 0.96 and 0.99, with a maximum RMSEP of 0.10 MPa. The prediction of fully relaxed RTS was possible using PLS-predicted density profiles of relaxing compacts. While compression levels present in the calibration were rather well predicted, significant biases at 11.9 and 16.8 kN compression forces were observed; including more compression levels in the calibration set would most likely fix this problem. An increase in the error was observed with an increasing compaction force for the four-component formulation only. This error could be explained by the nature of relaxing phenomena, more extreme and less repeatable at higher compression forces (creating more localized phenomena) that generated noise in the calibration model,

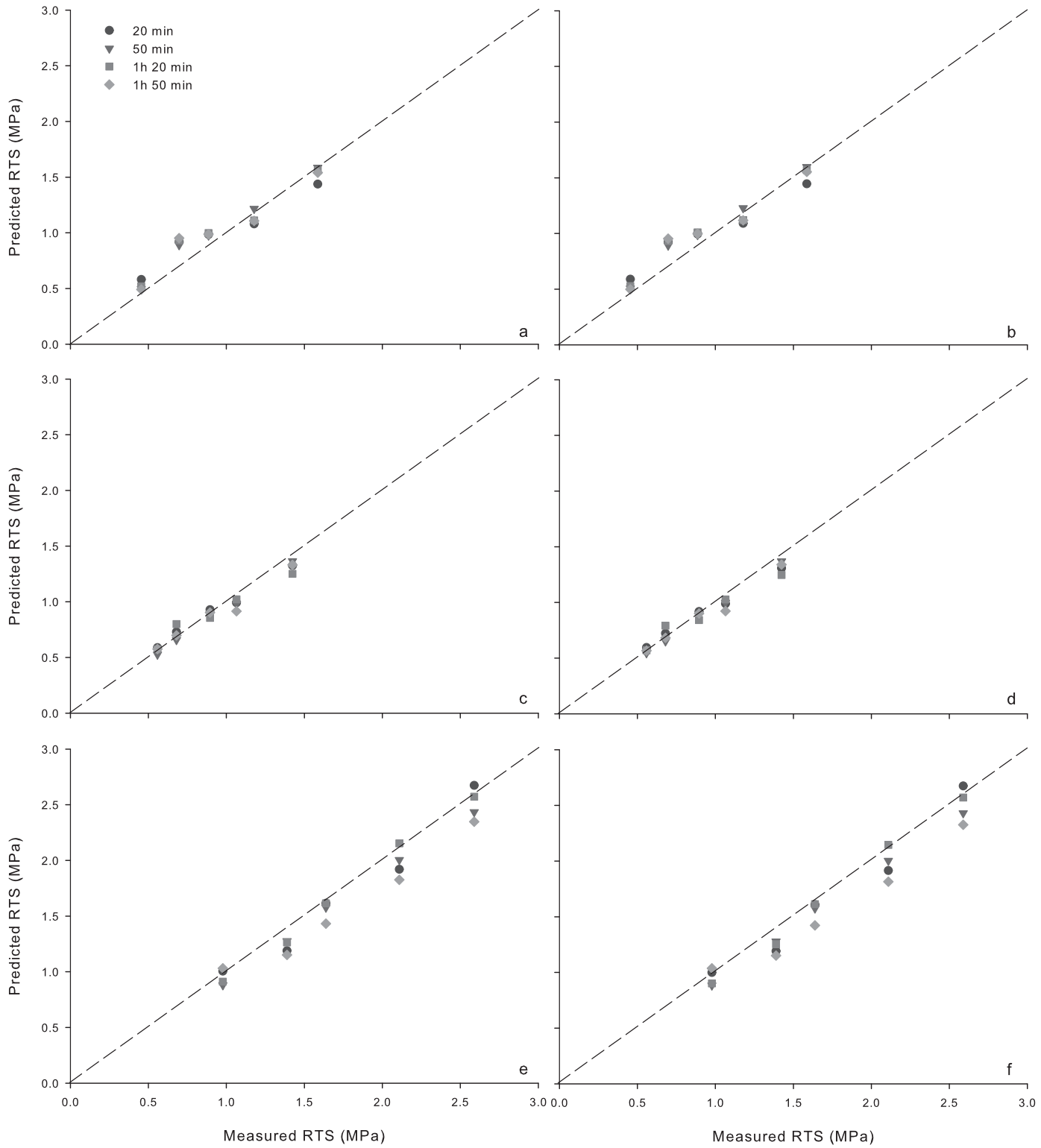

Fig. 4. Predicted vs. measured radial tensile strength for all three materials (starch (a and b), lactose (c and d), and the four-component formulation (e and f)) when dependent variables in the partial least squares model were measured after 20 min compression (a, c, and e) and 2 weeks (b, d, and f).

and by the fact that the formulation expressed different forms of relaxation compared to pure powder compacts.

No significant difference was observed between models developed on PLS-predicted density values calculated from density measurements made 20 min after compression (Fig. 4a, c, and e) and those using fully relaxed density measurements (Fig. 4b, d, and f). This was expected, as only a bias existed between the predicted median density values. An example of this phenomenon can be seen in Table 2 as a bias of 0.0137 mg mm^{-3} existed between both distributions. Biases of similar amplitudes were observed for other compression forces and were a function of the relaxation properties of each formulation. Powders with a greater tendency to change over time (those that relax more) demonstrated a greater bias. For example, the four-component formulation demonstrated

Table 2
Statistics of the density distribution of a starch compact compressed at 14.1 kN (mg mm^{-3}).

	Min	Max	Median	Mean	Stdev	Q^a 0.025	Q^a 0.25	Q^a 0.75	Q^a 0.975	Skewness	Kurtosis
Measured density after 2 weeks											
20 min	1.0330	1.3297	1.1857	1.1853	0.0257	1.1328	1.1703	1.2015	1.2340	-0.3648	4.9470
50 min	0.9454	1.3141	1.1852	1.1846	0.0262	1.1286	1.1698	1.2012	1.2329	-0.6610	6.2002
1 h 20 min	0.9652	1.3223	1.1873	1.1866	0.0263	1.1315	1.1714	1.2029	1.2363	-0.4781	5.2032
1 h 50 min	1.0268	1.3264	1.1866	1.1859	0.0270	1.1275	1.1708	1.2027	1.2359	-0.5639	5.1952
2 weeks	1.0505	1.5811	1.1735	1.1732	0.0287	1.1126	1.1557	1.1919	1.2267	-0.0453	6.2621
Measured density after 20 min											
20 min	1.0551	1.3371	1.1993	1.1990	0.0249	1.1481	1.1845	1.2146	1.2462	-0.3693	4.9577
50 min	0.9241	1.3241	1.1987	1.1981	0.0254	1.1437	1.1838	1.2141	1.2448	-0.6531	6.1232
1 h 20 min	0.9932	1.3320	1.2006	1.2000	0.0255	1.1466	1.1853	1.2158	1.2482	-0.4694	5.1657
1 h 50 min	1.0457	1.3357	1.2001	1.1995	0.0262	1.1432	1.1849	1.2157	1.2479	-0.5600	5.1875
2 weeks	1.0692	1.5814	1.1883	1.1881	0.0279	1.1292	1.1711	1.2063	1.2403	-0.0459	6.1792

[a] Quartile.

a bias of 0.0045 mg mm^{-3} compared to a 0.002 mg mm^{-3} bias for lactose.

Finally, the prediction of RTS from fully relaxed compacts (after 2 weeks) was demonstrated using the proposed approach. Observed r^2 of 0.99/0.99/0.97 and RMSEPs of 0.12/0.04/0.09 MPa for starch, lactose and the formulation respectively, were very similar to the results obtained for relaxing compacts.

3.3. Dynamics of relaxation

The potential to collect images of the same compact several times during the relaxation process without repositioning allows for the study of the relaxation dynamics. Fig. 5 presents difference images and histograms of starch compacts compressed at 14.1 kN for time 1 (20 min) minus time 2 (50 min), time 1 (20 min) minus time 3 (1 h 20 min), and time 1 (20 min) minus time 4 (1 h 50 min). Since compacts were not repositioned between collection times, it was possible to obtain density differences for each pixel at different collection times. Significant changes took place between each collection times, with for the present case, skewness and kurtosis being significantly affected (skewness: −4.93, −3.26, and −0.55; kurtosis: 132.08, 86.69, and 9.77). These trends were consistent from compression force to compression force and from material to material. Starch compacts compressed at 10 and 20 kN showed similar trends in those distribution moments but with different magnitudes.

While no other CQAs were investigated in the present article, studies of the relationship between the dynamics of relaxation and other compact properties such as dissolution profiles and disintegration times could help explain powder behavior. In addition, the local information provided by chemical imaging can allow the study of local phenomena within each compact and their impact on compact drug release and ultimately treatment efficacy and patient safety.

4. Discussion

The relationship between chemical imaging signal and radial tensile strength was determined in controlled conditions with low compression speed and following the initial post-ejection relaxation. While time scales of the process may vary from commercial tablet manufacturing conditions, this study establishes the ability of the technique and analysis to assess an important characteristic of the process. Further work needs to be done to determine if the methodology is sensitive enough as-is for the full-scale processes or if further refinement is required. However, the use of a production scale tablet press is not expected to change the observed phenomena. While the dynamics of relaxation might be different due to different compression mechanisms, it is expected that the density distribution is related to RTS in a manner similar to the present study.

Further method refinement may require adjustments to the timing of the analysis and the models. It is expected that the method

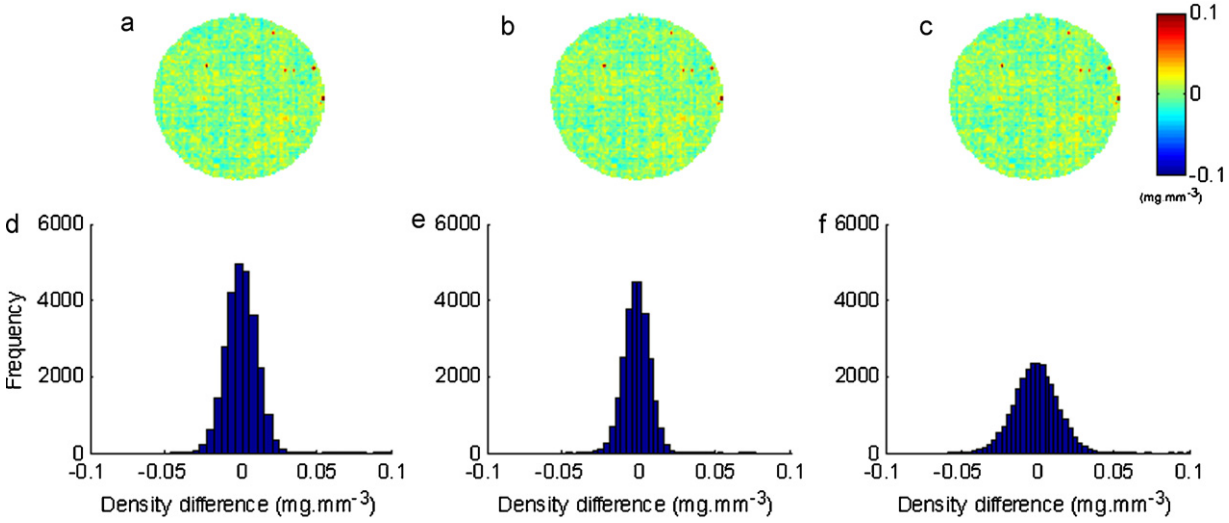

Fig. 5. Density difference images and their corresponding distributions for a starch compact compressed at 14.1 kN. (a) and (f) correspond to the difference between the images collected at time 1 (20 min) and time 2 (50 min), (b) and (e) correspond to the difference between the images collected at time 1 and time 3 (1 h 20 min), and (c) and (f) correspond to the difference between the images collected at time 1 and time 4 (1 h 50 min).

will be sensitive to the time between compression and data collection. Therefore, measurements must be performed at a consistent time after compression as the rate of relaxation is expected to be of greater amplitude. The median of the density distribution might need to be complemented with other statistics, such as the standard deviation or the skewness/kurtosis. These additional statistics are expected to take into account the shape of the rapidly changing density distribution. Specifically, it is anticipated that the more rapidly the tablet is relaxing, the more sensitive the prediction of RTS will be to the initial shape of the density distribution. For more plastically deformed materials present, the slower the relaxation and consequently, the mean or median of the distribution will be highly indicative of the equilibrium state of the tablet.

Near infrared chemical imaging is often considered a surface measurement method. Thus, relating bulk tablet properties such as RTS to surface density distribution might be highly dependent on the reproducibility of the compaction method employed. The literature on depth of penetration does not agree and a discrepancy exists between empirical (Cho et al., 1997) and simulated results (Clarke et al., 2002). Light penetration is a function of the wavelength, the particle size, and the density of the material. Recent simulated results demonstrate that significant contributions to the spectral data come from depths of up to 2.2 mm, based on the wavelengths used in this study (Shi and Anderson, 2010). Sampling performed as deep as 2.2 mm allows the characterization of the density information of not only the surface but also the bulk of the tablet. Thus, the use of chemical imaging for RTS prediction is relevant and reflects the density information of a significant volume of the tablet.

5. Conclusions

The prediction of radial tensile strength of solid dosage forms by near-infrared hyperspectral chemical imaging was studied. A two step process, involving the prediction of compact density at each pixel followed by the determination of the relationship between compact density distributions and RTS was implemented. Three formulations with varying relaxation properties were used. The density distributions of relaxing and relaxed compacts were found to be highly correlated to RTS of fully relaxed compacts. These results demonstrate the potential to use near-infrared chemical imaging to obtain RTS values for fully relaxed tablets. The implementation and the adaptation of such system is expected to help promote real-time release as the significant dimensionality reduction in data treatment offered by the approach allows high throughput cameras to be used for the determination of various chemical and physical tablet properties.

Acknowledgement

The authors wish to acknowledge Dr Peter L.D. Wildfong and Ira S. Buckner for their help in the physical design of the experiment. Authors would also like to thank Rahul Roopwani for his help with compression and radial tensile strength measurements.

References

Alam, A.S., Parrott, E.L., 1971. Effect of aging on some physical properties of hydrochlorothiazide tablets. J. Pharm. Sci. 60, 263–266.
Bakeev, K.A., 2005. Process Analytical Technology. Blackwell Publishing, Oxford.
Blanco, M., Alcalá, M., 2006a. Content uniformity and tablet hardness testing of intact pharmaceutical tablets by near infrared spectroscopy. A contribution to process analytical technologies. Anal. Chim. Acta 557, 353–359.
Blanco, M., Alcalá, M., González, J.M., Torras, E., 2006b. A process analytical technology approach based on near infrared spectroscopy: tablet hardness, content uniformity, and dissolution test measurements of intact tablets. J. Pharm. Sci. 95, 2137–2142.
Cao, X., Morganti, M., Hancock, B.C., Masterson, V.M., 2010. Correlating particle hardness with powder compaction performance. J. Pharm. Sci. 99, 4309–4316.
Cho, J.H., Gemperline, P.J., Aldridge, P.K., Sekulic, S.S., 1997. Effective mass sampled by NIR fiber-optic reflectance probes in blending process. Anal. Chim. Acta 348, 303–310.
Clarke, F.C., Hammond, S.V., Jee, R.D., Moffat, A.C., 2002. Determination of the information depth and sample size for the analysis of pharmaceutical materials using reflectance near-infrared microscopy. Appl. Spectrosc. 56, 1475–1483.
Cogdill, R.P., Anderson, C.A., Drennen, J.K., 2004. Using NIR spectroscopy as an integrated PAT tool. Spectroscopy 19, 104–109.
David, S.T., Augsburger, L.L., 1977. Plastic flow during compression of directly compressible fillers and its effect on tablet strength. J. Pharm. Sci. 66, 155–159.
Donoso, M., Kildsig, D.O., Ghaly, E.S., 2003. Prediction of tablet hardness and porosity using near-infrared diffuse reflectance spectroscopy as a nondestructive method. Pharm. Dev. Technol. 8, 357–366.
Ebube, N.K., Thosar, S.S., Roberts, R.A., Kemper, M.S., Rubinovitz, R., Martin, D.L., Reier, G.E., Wheatley, T.A., Shukla, A.J., 1999. Application of near-infrared spectroscopy for nondestructive analysis of Avicelò powders and tablets. Pharm. Dev. Technol. 4, 19–26.
Ellison, C.D., Ennis, B.J., Hamad, M.L., Lyon, R.C., 2008. Measuring the distribution of density and tableting force in pharmaceutical tablets by chemical imaging. J. Pharm. Biomed. Anal. 48, 1–7.
Fell, J.T., Newton, J.M., 1970. Determination of tablet strength by diametral compression test. J. Pharm. Sci. 59, 688–691.
Gendrina, C., Roggoa, Y., Collet, C., 2008. Pharmaceutical applications of vibrational chemical imaging and chemometrics: a review. J. Pharm. Biomed. Anal. 48, 533–553.
Gordon, M.S., Rudraraju, V.S., Rhie, J.K., Chowhan, Z.T., 1993. Effect of aging on the dissolution of wet granulated tablets containing super disintegrants. Int. J. Pharm. 97, 119–131.
Gowen, A.A., O'Donnell, C.P., Cullen, P.J., Bell, S.E.J., 2008. Recent applications of chemical imaging to pharmaceutical process monitoring and quality control. Eur. J. Pharm. Biopharm. 69, 10–22.
Guo, J.H., Skinner, G.W., Harcum, W.W., Malone, J.P., Weyer, L.G., 1999. Application of near-infrared spectroscopy in the pharmaceutical solid dosage form. Drug Dev. Ind. Pharm. 25, 1267–1270.
Gustafsson, C., Nystrom, C., Lennholm, H., Bonferoni, M.C., Caramella, C.M., 2003. Characteristics of hydroxypropyl methylcellulose influencing compatibility and prediction of particle and tablet properties by infrared spectroscopy. J. Pharm. Sci. 92, 494–504.
Parris, J., Airiau, C., Escott, R., Rydzak, J., Crocombe, R., 2005. Monitoring API drying operations by NIR. Spectroscopy 20, 34–42.
Karehill, P.G., Nystrom, C., 1990. Studies on direct compression of tablets. Part 2. Investigation of strength increase upon aging and bonding mechanisms for some plastically deforming materials. Int. J. Pharm. 64, 27–34.
Kirsch, J.D., Drennen, J.K., 1999. Nondestructive tablet hardness testing by near-infrared spectroscopy: a new and robust spectral best-fit algorithm. J. Pharm. Biomed. Anal. 19, 351–362.
Lordi, N., Shiromani, P., 1984. Mechanism of hardness of aged compacts. Drug Dev. Ind. Pharm. 10, 729–752.
Lowenthal, W., 1972. Disintegration of tablets. J. Pharm. Sci. 61, 1695–1711.
Morisseau, K.M., Rhodes, C.T., 1997. Near-infrared spectroscopy as a nondestructive alternative to conventional tablet hardness testing. Pharm. Res. 14, 108–111.
Otsuka, M., Yamane, I., 2006. Prediction of tablet hardness based on near infrared spectra of raw mixed powders by chemometrics. J. Pharm. Sci. 95, 1425–1433.
Rees, E., Shotton, E., 1970. Some observations on the aging of sodium chloride compacts. J. Pharm. Sci. 22, 17S–23S.
Reich, G., 2005. Near-infrared spectroscopy and imaging: basic principles and pharmaceutical applications. Adv. Drug Deliv. Rev. 57, 1109–1143.
Roggo, Y., Chalus, P., Maurer, L., Lema-Martinez, C., Edmond, A., Jent, N., 2007. A review of near infrared spectroscopy and chemometrics in pharmaceutical technologies. J. Pharm. Biomed. Anal. 44, 683–700.
Roggo, Y., Roeseler, C., Ulmschneider, M., 2004. Near infrared spectroscopy for qualitative comparison of pharmaceutical batches. J. Pharm. Biomed. Anal. 36, 777–786.
Sarraguca, M.C., Lopes, J.A., 2009. Quality control of pharmaceuticals with NIR: from lab to process line. Vibr. Spectrosc. 49, 204–210.
Shi, Z., Anderson, C.A., 2010. Application of Monte Carlo simulation-based photon migration for enhanced understanding of near-infrared (NIR) diffuse reflectance. Part I. Depth of penetration in pharmaceutical materials. J. Pharm. Sci. 99, 2399–2412.
Shi, Z., Cogdill, R.P., Short, S.M., Anderson, C.A., 2008. Process characterization of powder blending by near-infrared spectroscopy: blend end-points and beyond. J. Pharm. Biomed. Anal. 47, 738–745.
Short, S.M., Cogdill, R.P., Wildfong, P.L.D., Drennen, J.K., Anderson, C.A., 2009. A near-infrared spectroscopic investigation of relative density and crushing strength in four-component compacts. J. Pharm. Sci. 98, 1095–1109.
Swarbrick, B., Grouta, B., Noss, J., 2005. The rapid, at-line determination of starch content in sucrose–starch blends using near-infrared reflectance spectroscopy; a process analytical technology initiative. J. Near Infrared Spectrosc. 13, 1–8.
Tatavarti, A.S., Fahmy, R., Wu, H., Hussain, A.S., Marnane, W., Bensley, D., Hollenbeck, G., Hoag, S.W., 2005. Assessment of NIR spectroscopy for nondestructive analysis of physical and chemical attributes of sulfamethazine bolus dosage forms. AAPS PharmSciTech. 6, E91–E99.
Wu, C.Y., Best, S.M., Bentham, A.C., Hancock, B.C., Bonfield, W., 2006. Predicting the tensile strength of compacted multi-component mixtures of pharmaceutical powders. Pharm. Res. 23, 1898–1905.